Journal of Marine Systems 83 (2010) 141–149

Contents lists available at ScienceDirect

Journal of Marine Systems

journal homepage: www.elsevier.com/locate/jmarsys

# Winter phytoplankton bloom induced by subsurface upwelling and mixed layer entrainment southwest of Luzon Strait

JiuJuan Wang [a,b], DanLing Tang [a,b,*], Yi Sui [c]

[a] Research Center of Remote Sensing and Marine Ecology & Environment (RSMEE), LED, South China Sea Institute of Oceanology, Chinese Academy of Sciences, 164 West Xingang Road, Guangzhou, 510301, PR China
[b] Graduate University of Chinese Academy of Sciences, Beijing 100049, PR China
[c] Department of Oceanography, College of Physical and Environmental Oceanography, Ocean University of China, 5 Yushan Road, Qingdao, PR China

ARTICLE INFO

*Article history:*
Received 11 September 2009
Received in revised form 5 May 2010
Accepted 9 May 2010
Available online 17 May 2010

*Keywords:*
Winter phytoplankton bloom
Subsurface upwelling
Entrainment
Wind
South China Sea

ABSTRACT

Phytoplankton blooms appear in winter (Nov–Jan) in the southwest of Luzon Strait, South China Sea, which is an oligotrophic region in general. To understand dynamic features of the winter phytoplankton bloom southwest of Luzon Strait, this study analyzes seven years (2000–2006) of remote sensing data of Chlorophyll *a*, sea surface temperature, and ocean vector winds, along with *in situ* observations of dissolved oxygen, nutrients (nitrate, phosphate, and silicate), and physical oceanographic parameters mixed layer depth, Ekman pumping velocity, and entrainment velocity. The results demonstrate that the winter phytoplankton bloom in the southwest of Luzon Strait is primarily induced by both Ekman pumping-driven upwelling (observed at about 50 m under sea surface) and upper mixed layer entrainment. The area of winter phytoplankton blooms is about $2.58\times10^4$ km$^2$, based on Empirical Orthogonal Function analysis. The seasonal variability of the bloom is associated with monsoonal wind forcing.



## 1. Introduction

The South China Sea (SCS) is the largest marginal sea in the western tropical Pacific. Several oceanographic studies of the SCS are related to Luzon Strait which connects the Western Pacific Ocean to the SCS (Fig. 1A), including Kuroshio intrusion (Farris and Wimbush, 1996), mesoscale eddies (Wu and Chiang, 2007), and internal waves (Liu and Hsu, 2003). The hydrological characteristics of Luzon Strait are complex and influenced by the general condition of the SCS, which is in turn influenced by the Asian monsoon system. This system neighbors four monsoon subsystems: the subtropical East Asian monsoon, the tropical Indian monsoon, the Western North Pacific monsoon, and the Australian monsoon (Wang et al., 2009). Northeast monsoon winds over the SCS blow in winter at a mean speed of 9 m s$^{-1}$; southwest monsoon winds with an average speed of 6 m s$^{-1}$ prevail during the summer period (Wyrtki, 1961).

Though the SCS is a relatively oligotrophic tropical–subtropical ocean (Tang et al., 1999, 2004b), winter phytoplankton blooms occur in the vicinity of Luzon Strait in certain years (Tang et al., 1999; Chen et al., 2006; Peñaflor et al., 2007). Tang et al. (1999) first reported this phenomenon appeared in the winters of 1981, 1982 and 1984 using Coastal Zone Color Scan (CZCS) data. Using Moderate Resolution Imaging Spectroradiometer (MODIS)-derived data, Peñaflor et al. (2007) indicated the presence of blooms southwest of Luzon Strait in the winters of 2003 and 2004. Prior studies have suggested upwelling can be responsible for the winter phytoplankton blooms southwest of Luzon Strait. Winter upwelling brings nutrients from deeper layers closer to the surface, fueling phytoplankton blooms (Tang et al., 1999; Chen et al., 2006; Peñaflor et al., 2007). The winter upwelling near Luzon Strait does not have a strong sea surface manifestation. As such, the upwelling is difficult to detect from satellite-derived sea surface temperature (SST) images (Udarbe-Walker and Villanoy, 2001). Shaw et al. (1996) initially reported this winter upwelling, pointing out that the upwelling in this area was affected by a remotely forced component arising from the basin-wide gyre circulation. However, Shaw's results were based on only one cruise in December, 1990. Using numerical modeling, Chao et al. (1996) noted that the upwelling was associated with inflow of Pacific water during winter. Qu (2000) argued that wind stress curl might play a major role in generating the winter upwelling off Luzon Strait based on computations of the wind stress curl and its seasonal variability.

Hydrological conditions near Luzon Strait are complex, and the related environmental variability may influence biological processes. Peñaflor et al. (2007) described winter phytoplankton blooms on the west side of Kuroshio front. They related these blooms to the northward-flowing Luzon coastal current and a westward intrusion of the Kuroshio during Northeast monsoon. The surface inflow of Kuroshio water from the western Philippines is about $2.7\times10^{-1}$ km$^3$ year$^{-1}$ (Chen et al., 2003). The intrusion of the Kuroshio results in mesoscale

* Corresponding author. Research Center of Remote Sensing & Marine Ecology Environment (RSMEE), LED, South China Sea Institute of Oceanology, Chinese Academy of Sciences, 164 West Xingang Road, Guangzhou, 510301, PR China. Tel./fax: +86 20 89023203.
*E-mail address:* lingzistdl@126.com (D. Tang).
*URL:* http://lingzis.51.net/index.html (D. Tang).

0924-7963/$ – see front matter © 2010 Elsevier B.V. All rights reserved.
doi:10.1016/j.jmarsys.2010.05.006

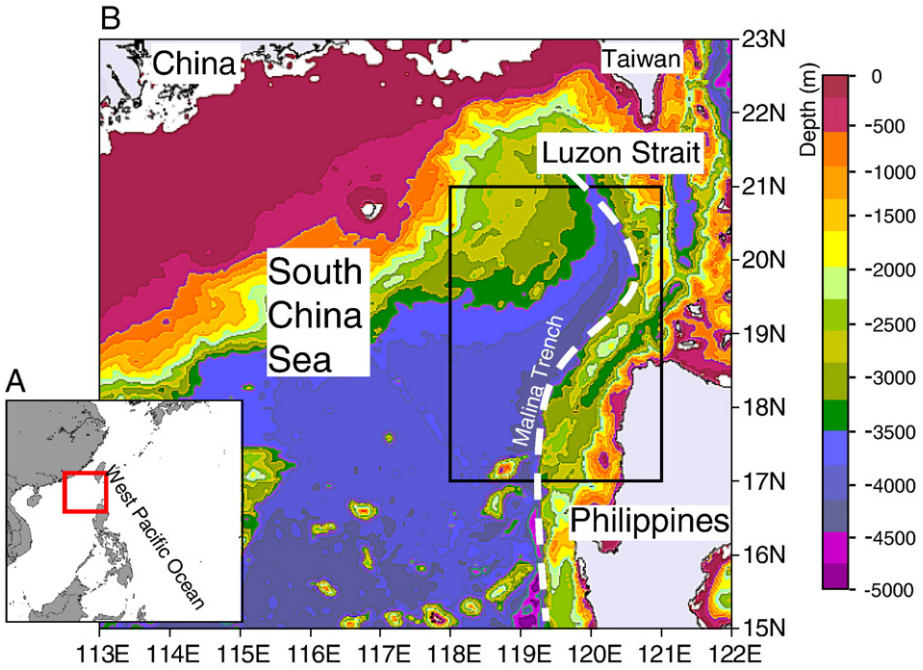


**Fig. 1.** A. Location of study area. The red line box indicates the enlarged area of B; B. Map of the study area (black bold line box) in SCS. The white dash indicates the Malina Trench. Color shading indicates bathymetry.

eddies in the vicinity of Luzon Strait (Wu and Chiang, 2007). The dynamics of mesoscale eddies influences biogeochemical budgets in the upper ocean (McGillicuddy et al., 1999). Vertical nutrient flux can be induced by mesoscale eddies, leading to enhanced new production (McGillicuddy and Robinson, 1997; McGillicuddy et al., 1998). Chen et al. (2007) investigated the biological and chemical effects of a cold-core eddy that was shed from the Kuroshio Current at the Luzon Strait during April to May of 2005. They indicated that cold core eddies were intermittently formed all year round as the Kuroshio invades the SCS, and their effects on phytoplankton productivity and community assemblages are likely to have important influences on biogeochemical cycling in the region. Tides, internal waves, and typhoons may also contribute to the regional winter phytoplankton blooms (Chen et al., 2006). However, previous reports have been constrained by short time-series, which were only able to reflect the relationship between the bloom and the particular environmental situation in each specific year.

Here we combine remote sensing and statistical analysis in a long-term study to investigate the variability of oceanic phenomenon (e.g. seasonal or inter-annual fluctuations and the spatial distributions) and provide insight into the marine biological processes (cf. Peliz and Fiúza, 1999; Steinberg et al., 2001; Radiarta and Saitoh, 2008). The present work provides a comprehensive description of the phytoplankton blooms southwest of Luzon Strait in winter conditions using 7 years of satellite-derived data, *in situ* biological and chemical observations, and physical oceanographic parameters. Our aims are to a) characterize the spatio-temporal patterns of the phytoplankton blooms in southwestern Luzon Strait with statistical model and specify the region in which phytoplankton blooms occur; b) investigate the controlling factors of the timing, intensity and location of the blooms by long-term analysis; c) present a conceptual model to depict the mechanism responsible for the winter blooms near Luzon Strait.

## 2. Methods

### 2.1. Study area

The study area (Fig. 1B) is situated at 118.0°E–121.0°E, 17.0°N–21.0°N along part of Malina trench, which reaches depths of about 5000 m, but the average depth of the SCS is only about 1500 m (Hayes and Lewis, 1984). The area is affected by the northeast monsoon in winter and southwest monsoon in summer (Shaw and Chao, 1994). The wind has influence on the local marine ecosystem (Tang et al., 1999).

### 2.2. Satellite-derived data

Sea surface Chlorophyll *a* (Chl *a*) concentration data were derived from the Sea-viewing Wide Field of view Sensor (SeaWiFS) launched in 1997 and MODIS Aqua launched in 1999. The data were obtained from the Distributed Active Archive Centre (DAAC), NASA (http://oceancolor.gsfc.nasa.gov/). Monthly averaged Chl *a* images of MODIS Aqua in 2005 were processed for the study area, then individual scenes were composited into seasonal mean Chl *a* images using a cylindrical projection with the SeaWiFS Data Analysis System (SeaDAS 5.3). SeaWiFS monthly 9-km resolution data from January 2000 to December 2006 were used for statistical analysis.

Satellite-derived sea surface temperature (SST) data were processed from MODIS Aqua. The seasonally averaged MODIS SST images corresponded to the Chl *a* images from 2005 utilized in this study.

Ocean vector wind data were retrieved from QuikSCAT, a polar orbiting satellite with an 1800 km wide measurement swath on the earth's surface (http://winds.jpl.nasa.gov/missions/quikscat/index.cfm). Gridded data (0.25° resolution) from 2000 to 2006 were analyzed to investigate the temporal and spatial variability in the study region.

### 2.3. Mixed layer depth, Ekman pumping velocity and entrainment velocity

The ocean mixed layer is the top layer where temperature and salinity are vertically well-mixed. The uniformity of the mixed layer is due primarily to mixing processes caused by winds and fluxes of heat and fresh water. Time series data of monthly mean mixed layer depth for the study area from January 2000 to December 2006 were produced with the Giovanni online data system, developed and maintained by the NASA Goddard Earth Sciences (GES) Data and Information Services Center (DISC).

We also analyzed output from the NASA Ocean Biogeochemical Model (NOBM). The NOBM is a coupled three-dimensional model incorporating general circulation, biogeochemical, and radiative components. The output data products from the NOBM available for analysis in Giovanni are: total chlorophyll, diatoms, chlorophytes, cyanobacteria, coccolithophores, nitrate, and mixed layer depth. The forcing inputs to the model are provided by National Center for Environmental Prediction (NCEP) Reanalysis, Optimally Interpolated Sea Surface Temperature (OISST), Goddard Chemistry Aerosol Radiation and Transport (GOCART), Total Ozone Mapping Spectrometer (TOMS), and International Satellite Cloud Climatology Project (ISCCP) (http://gdata1.sci.gsfc.nasa.gov/daac-bin/G3/gui.cgi?instance_id=ocean_model).

To calculate monthly average Ekman pumping velocity for 2005, we first determined the months when winds were from the northeast (i.e. upwelling favorable wind; $Curl\ (\tau)<0$). Then the Ekman pumping velocity was calculated from wind stress ($\tau$) from January to April and October to December when the winds were upwelling favorable. The Ekman pumping velocity ($W_E$) can be estimated to be as follows:

$$\tau = \rho_a C_d U_{10}^2 \quad (1)$$

$$W_E = -Curl_z\left(\frac{\tau}{\rho_w f}\right) \quad (2)$$

where $\rho_a$ is the density of air (1.25 kg m$^{-3}$), $\rho_w$ is the density of seawater (1025 kg m$^{-3}$), $C_d$ is the drag coefficient ($2.6\times10^{-3}$), $U_{10}$ is the wind speed 10 m above sea level, and $f$ is the Coriolis parameter ($5.39\times10^{-5}$ s$^{-1}$ at 18.5°N) (Stewart, 2008).

The entrainment velocity ($W_e$) is associated with mixed layer depth ($h$) deepening and modified by Ekman pumping velocity ($W_E$) (Alexander, 1992; Mendoza et al., 2005). It can be expressed as:

$$W_e = \left(\frac{\partial h}{\partial t} - W_E\right) \quad (3)$$

### 2.4. In situ observations

Climatological means of dissolved oxygen (DO), and nutrients (phosphate (P), silicate (Si), and nitrate (N)) were retrieved from the World Ocean Atlas 2005 (WOA05) hydrographic database of the National Oceanographic Data Center (NODC). WOA05 provides monthly climatologies of temperature (Locarnini et al., 2006), salinity (Antonov et al., 2006), DO, apparent oxygen utilization, oxygen saturation (Garcia et al., 2006a), and dissolved inorganic nutrients (Garcia et al., 2006b) at standard depth levels (0, 10, 20, 30, 50, 75, 100, 125, 150, 200, 250, 300, 400 m,..., 1500 m). In this database, oceanographic temperature profile data were from bottle samples, Mechanical Bathythermograph (MBT), Conductivity–Temperature–Depth (CTD) instruments, Digital Bathythermograph (DBT), Expendable Bathythermograph (XBT), profiling floats, moored and drifting buoys, gliders, and undulating oceanographic recorder (UOR) profiles (Locarnini et al., 2006). All of the quality-controlled $O_2$ and nutrient data used in the WOA05 were obtained by serial (discrete) water column samples (Garcia et al., 2006b). The $O_2$ values were analyzed by various modifications of the Winkler titration method using visual, amperometric, or photometric end-detections. The nutrient data consisted of individual stations containing 1 to 36 water samples collected at various depths between the surface and the ocean bottom using Nansen or Niskin bottles (Garcia et al., 2006b).

### 2.5. Empirical Orthogonal Function analysis

Empirical Orthogonal Function (EOF) analysis is a technique to identify prominent patterns of variance from a given data set (Kutzbach, 1967; Hardy, 1977). It is also referred to as Principal Component Analysis (PCA), and this technique has a long history of application to meteorological data (Lorenz, 1956). EOF analysis enables fields of highly correlated data to be represented adequately by small number of orthogonal functions and a corresponding time-series of coefficients (Weare et al., 1976). This method provides an effective means to identify the dominant spatial and temporal patterns from series of remote sensing data (Nezlin and McWilliams, 2003; Emilie and Francis, 2009). In this study, the EOF approach is applied to analysis of remote sensing Chl *a* data of the study area (Fig. 1) from 2000 to 2006.

## 3. Results

### 3.1. Phytoplankton bloom area

EOF analysis reveals the typical offshore pattern (Fig. 2A and B) and seasonal cycle (Fig. 2C) of Chl *a* concentrations in the southwest of Luzon Strait. The first EOF mode accounts for 60.1% of the total variance, and the second mode accounts for 11.6%. Spatial patterns show patch of strong positive signal of Chl *a* concentrations centered at 119.0°E, 19.0°N covering an area of ca. $2.58\times10^4$ km$^2$ off the coast of northwest Philippines (Fig. 2A and B). Chl *a* concentrations exhibit a decreasing gradient (relatively weaker signal) around the patch. The lowest Chl *a* concentration with the weakest signal occurs at the entrance of Luzon Strait. The seasonal variability is reflected by the time-series of amplitudes (Fig. 2C) associated with the spatial pattern of the first mode (Fig. 2A). The positive signals with prominent peak of Chl *a* concentrations generally appear in winter each year.

### 3.2. Seasonal variations of Chl a, SST and surface winds

Seasonal variations of the phytoplankton blooms were depicted by averaged MODIS images of Chl *a* concentrations (Fig. 3A) from 2005. A bloom was detected southwest of Luzon Strait in winter (Nov–Jan), reflected by higher Chl *a* concentrations (>0.3 mg m$^{-3}$) than other three seasons (Fig. 3A). The location of this bloom centered at 118.5°E, 19.7°N coincides with the bloom region identified by EOF method (Fig. 2A). Fig. 3B shows SSTs are higher in summer and autumn than winter and spring. However, there was no discernable covariation between SST and Chl *a* in the bloom region (Fig. 3B.1).

Regional winds fluctuated in intensity and direction in different seasons (Fig. 3C). In winter (Nov–Jan), strong northeast winds of ca. 16 m s$^{-1}$ appeared at the entrance of Luzon Strait along the northwest tip of the Philippines (Fig. 3C.1). During summer (May–Jul), southwest wind in Luzon Strait was weaker than the wind to the north of Luzon Strait near Taiwan (Fig. 3C.3). Spring (Feb–April) and autumn (Aug–Oct) were transitional periods, and the wind conditions in these two seasons were relatively moderate with changing directions (Fig. 3C.2 and C.4). Fig. 4 shows the variations of spatially-averaged wind speed and direction in the study area for the period of 2000–2006, illustrating the prevailing northeast wind ca. 12 m s$^{-1}$ in winter and southwest ca. 4 m s$^{-1}$ in summer.

### 3.3. Fluctuations in Chl a, mixed layer depth, and wind speed

The time-series of spatial mean Chl *a* concentration coincided with mixed layer depth (Fig. 5A) and wind speed (Fig. 5B). Linear regression analysis reveals a high correlation coefficient ($r=0.83$, significant at the 95% confidence level) between Chl *a* concentration and mixed layer depth in the study region. The highest Chl *a* concentration (0.43 mg m$^{-3}$) is in winter and lowest in summer (0.08 mg m$^{-3}$). The mixed layer deepens in autumn, reaching a maximum about 60 m in winter. In spring, the mixed layer begins to shallow and reaches to a minimum of 12 m in summer (Fig. 5A). The strongest wind speed corresponding to the highest Chl *a* also appears in winter (Fig. 5B).

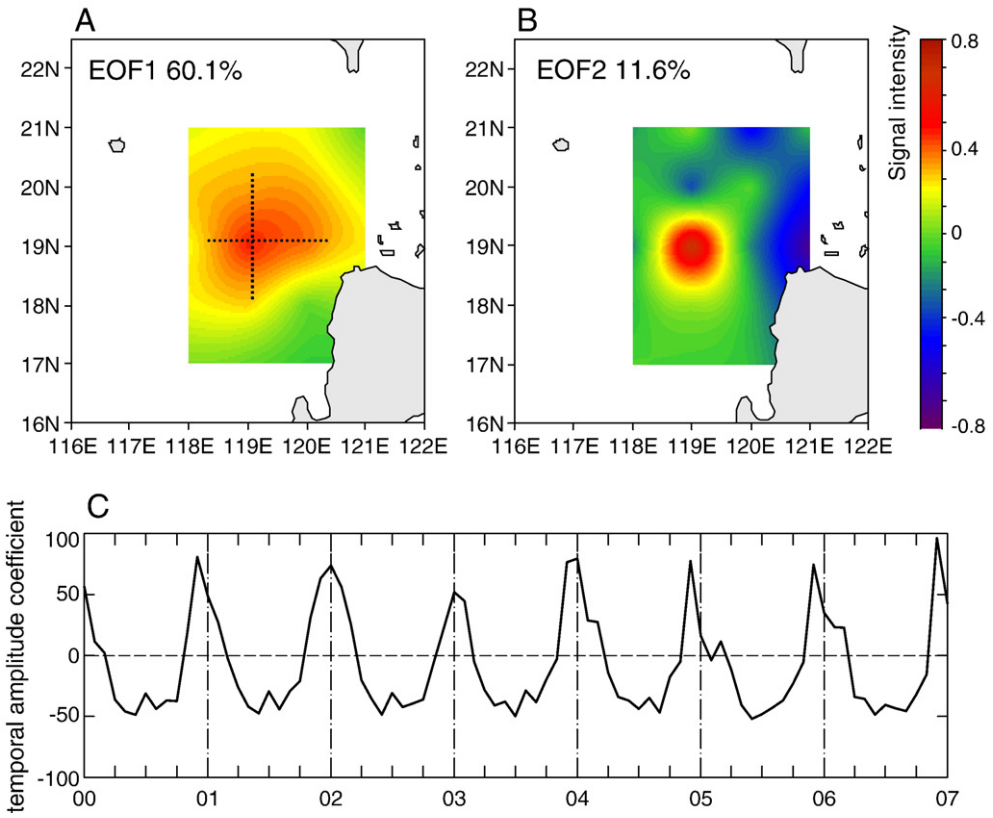


**Fig. 2.** A. Spatial pattern of the first EOF on Sea Surface Chl *a* data. Percentage of variance explained is 60.1%. The dotted cross shows the extent of phytoplankton bloom; B. Spatial pattern of the second EOF mode, which accounts for 11.6% of the total variance. The strong signal intensity in each mode indicates high Chl *a* concentrations consistently appear at this location; C. Time series of the amplitude of the first EOF mode.

### *3.4. Vertical variation of temperature, DO and nutrients (N, P and Si)*

Horizontal distributions of temperature were quite different in winter (December) and summer (June) in 2005 (Fig. 6). In winter, a cold temperature core appeared at 50 m depth in the study area along the northwest Philippine coast (Fig. 6C), and the feature was more obvious deeper in the water column (75 m) (Fig. 6D). At the depth of 0 m (Fig. 6A), 30 m (Fig. 6B), there were no signals of the cold water mass. In summer, sea temperature was relatively higher than in winter at each depth, and the winter cold temperature core was not present (Fig. 6E–F).

Fig. 7 illustrates the vertical profiles of DO, N, P and Si in December 2005 averaged from 10 stations located in the cold water core. The DO concentration in the upper mixed layer (58 m) ranged from 4.72 mg $L^{-1}$ to 4.58 mg $L^{-1}$. However, it varied from 4.58 mg $L^{-1}$ to 2.96 mg $L^{-1}$ below 50 m to 250 m (Fig. 7A). The profile of N (Fig. 7B) displayed a narrow fluctuation between 0.32 μM and 0.48 μM in the upper 58 m. Below the mixed layer depth, the concentration of N rapidly increased with depth, reaching a peak value of 13.08 μM at the depth of 250 m. The vertical profiles of P and Si concentrations showed similar trend to that of N. The concentration of P (Fig. 7C) was low throughout the mixed layer, ranging from 0.32 μM to 0.48 μM; a prominent increase with depth occurred between the mixed layer depth and 250 m. The Si profile (Fig. 7D) also displayed little variation within the mixed layer, and reached a maximum of 28.78 μM at 250 m depth.

### *3.5. Ekman pumping and entrainment*

In Fig. 8 monthly mean Ekman pumping velocity and entrainment velocity are compared in the months when the winds are from northeast (January to April and October to December). From May to September, southwest winds prevail, which are not upwelling favorable (data not shown here). The velocities of Ekman pumping and entrainment in January and December are two to five times higher than in other months and consistent with high Chl *a* concentrations in these months (Fig. 5). Both Ekman pumping and entrainment reach their highest values in December ($5.96\times10^{-5}$ m $s^{-1}$ and $6.07\times10^{-5}$ m $s^{-1}$, respectively). In October, Ekman pumping and entrainment are generally weak, but gradually increase with the onset of winter.

## 4. Discussion

### *4.1. The region of the phytoplankton blooms*

EOF analysis revealed the presence of winter phytoplankton blooms centered at 119.0°E, 19.0°N covering an area of ca. $2.58\times10^{4}$ $km^2$ (Fig. 2). Chl *a* is high in this region during winter off the northwest coast of the Philippines, in accordance with previous studies. High pigment concentration southwest of Luzon Strait was centered at 118.5°E, 19.0°N in December 1979 (Tang et al., 1999). The bloom also appeared in

**Fig. 3.** Seasonal images from 2005. A. MODIS-derived Chl *a* in (A.1) winter, (A.2) spring, (A.3) summer, (A.4) autumn. The ellipse indicates the location of the offshore bloom phenomena; B. MODIS-derived SST. The ellipse in B.1 shows no SST anomaly in the bloom region in winter; C. QuickScat wind. The small arrows indicate wind directions, and the color indicates wind speed.

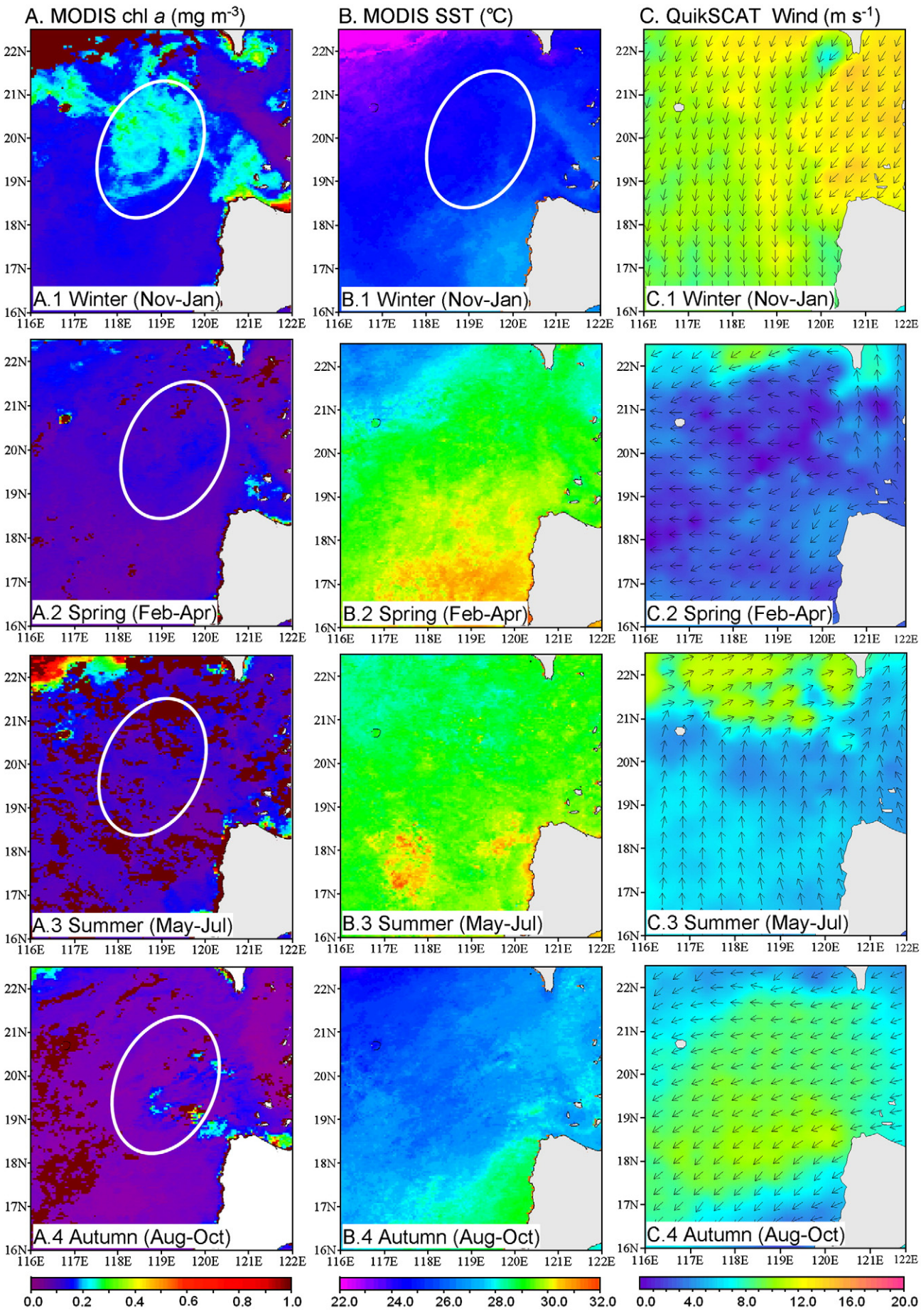

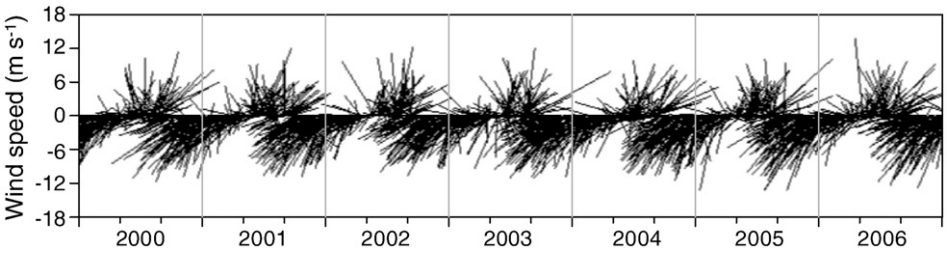


**Fig. 4.** Time series of wind speed and direction. The length of the stick indicates wind speed; the direction of the stick indicates wind direction.

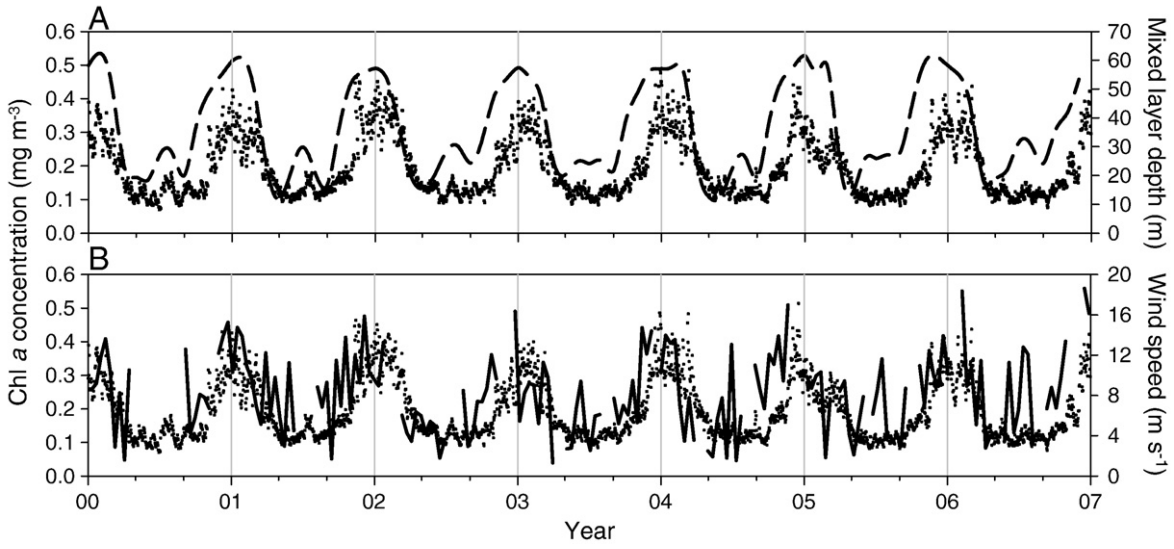


**Fig. 5.** Time series of (A) Chl *a* concentration and mixed layer depth from the NASA Ocean Biogeochemical Model (NOBM); (B) Chl *a* and QuickScat wind speed. Dots: Chl *a* concentration; dashed line: mixed layer depth; solid line: wind speed.

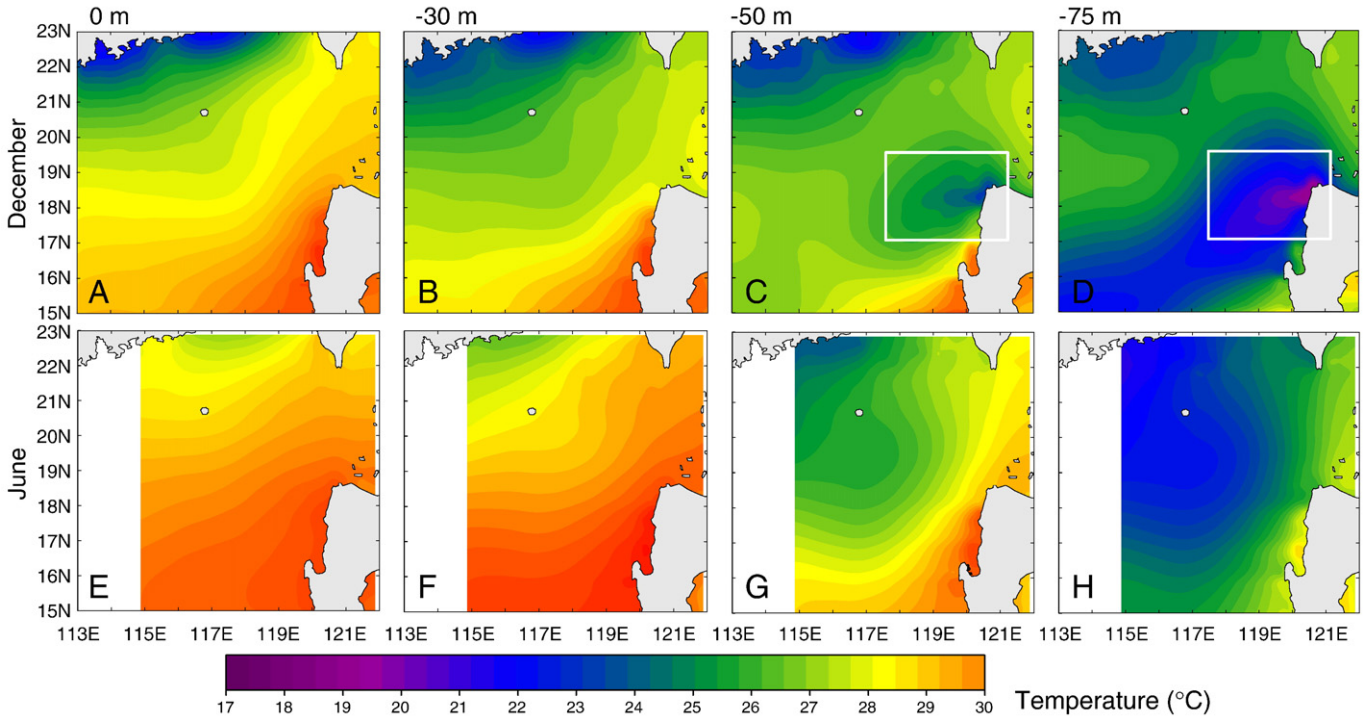


**Fig. 6.** Temperature distribution at 0 m, −30 m ,−50 m, −75 m depth in December (A–D) and June (E–H), 2005. The rectangles in C, D indicate the subsurface upwelling phenomenon. Temperature of each depth is from World Ocean Atlas 2005 (WOA05) of the National Oceanographic Data Center (NODC).

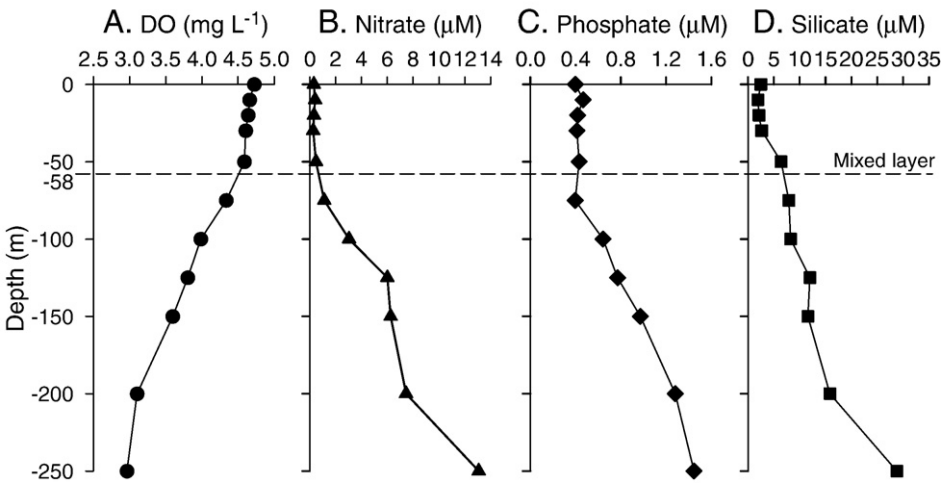


**Fig. 7.** Dissolved oxygen (DO) and nutrient profiles, December 2005. A. DO; B. Nitrate (N); C. Phosphate (P); and D. Silicate (Si) retrieved from World Ocean Atlas 2005 (WOA05) of the National Oceanographic Data Center (NODC). Dashed line: mixed layer depth in December, 2005 (58 m).

January 1983 centered at 119.0°E, 20.0°N. In December 2003, the bloom center was at 118.5°E, 19.5°N (Peñaflor et al., 2007).

Phytoplankton production in the ocean is normally limited by nutrient availability and solar radiation (Tang et al., 2004a; Siegel et al., 2007; Dwivedi et al., 2008). The study area is located in a relatively oligotrophic tropical–subtropical ocean (Tang et al., 1999, 2004b). Averaged winter SST of about 24.3 °C promotes the growth of phytoplankton (Peñaflor et al., 2007), and monthly mean photosynthetically active radiation (PAR) observed in winter at the study area is high (Chen et al., 2006). Thus, in this environment, phytoplankton growth is limited by nutrient availability rather than light and temperature (Tang et al., 1999). Therefore, the key to understanding the formation of the winter blooms lies in elucidation of the mechanisms of the nutrient supply to the upper layer.

### 4.2. Subsurface upwelling and mixed layer depth deepening during blooms

Upwelling regions are typically associated with high productivity due to transport of nutrient-rich deep water toward sea surface (Labiosal and Arrigo, 2003; Tang et al., 2004b; Wilkerson et al., 2006). Upwelling is reflected by cold sea surface temperature, low DO concentration, as well as negative sea level anomaly (Shaw et al., 1996; Tang et al., 2002; Collins et al., 2003; Martin and Villanoy, 2008).

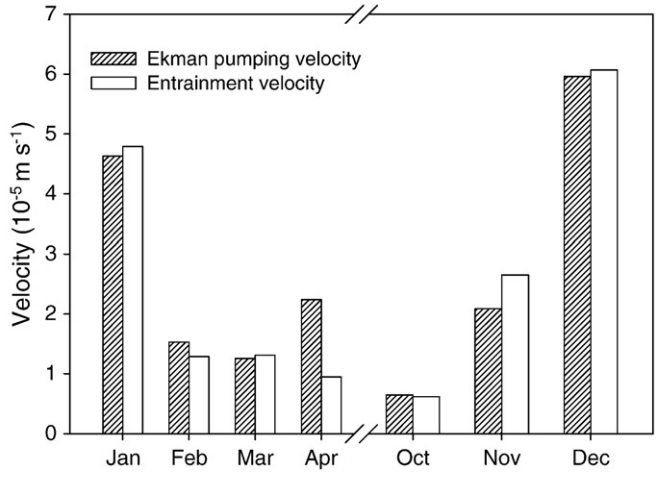


**Fig. 8.** Time-series of Ekman pumping velocity and entrainment velocity for the months when the winds are upwelling favorable. The calculations are based on wind stress and change of mixed layer depth.

However, southwest Luzon Strait appears to have significant differences from other classic upwelling regions, insofar as the upwelling is, for the most part, evident only in subsurface anomalies. The cold sea temperature mass (Fig. 6C) is only detected in winter at depths of 50 m and deeper; in summer it is difficult to observe this phenomenon (Fig. 6E–F). Low DO (Fig. 7A) and high nutrients (Fig. 7B–D) are also observed in the subsurface layer only in winter time. In the mixed layer, DO concentration varies within $\pm 0.07$ mg $L^{-1}$; below that, DO dramatically decreases from 4.58 mg $L^{-1}$ to 2.96 mg $L^{-1}$ at a depth of 250 m (Fig. 7A). Dissolved inorganic nutrients (N, P and Si) remain low in the mixed layer, implying that upwelled nutrients are not transported all the way to the surface (Fig. 7B–D). Because the amplitude of the upwelling is relatively weak, it is difficult to detect its signature in sea surface parameters, either by remote sensing or *in situ* measurement. However, upwelling is clearly evident in cold anomalies present in subsurface layers (Udarbe-Walker and Villanoy, 2001). Low sea level anomalies in the study region in wintertime are also consistent with upwelling (Martin and Villanoy, 2008). However, the high Chl *a* present in near-surface waters cannot be fully explained by subsurface upwelling, as it does not appear to transport nutrients all the way to the surface.

### 4.3. Mechanisms responsible for the offshore winter phytoplankton bloom

#### 4.3.1. Physical and biological processes

Wind events play an important role in physical and biological processes of the upper ocean (Tang et al., 2003; Botsford et al., 2006). Our results demonstrate that upwelling southwest of Luzon Strait is a subsurface phenomenon (Fig. 6) with low DO and high nutrients (Fig. 7). The upwelling depends on Ekman pumping associated northeast monsoonal wind.

Time series of local synoptic wind forcing indicate that winds in winter are much stronger than in summer (Fig. 4). The surface mixed layer in the study area deepens to more than 60 m during winter and becomes as shallow as 10 m to 20 m in summer in response to the monsoonal winds (Fig. 5). The strong winds during winter promote evaporative cooling to drive convective mixing in the upper ocean. The tendency of turbulence to diffuse into the adjoining non-turbulent layer leads to the erosion of the underlying stratification of the thermocline, thus increasing the mixed layer thickness via entrainment (Strang and Fernando, 2001; Backhaus et al., 2003; Labiosal and Arrigo, 2003).

During the period of high winds, both Ekman pumping and entrainment strengthen. In December and January, entrainment is slightly stronger than Ekman pumping (Fig. 8). The high concentrations of Chl *a*

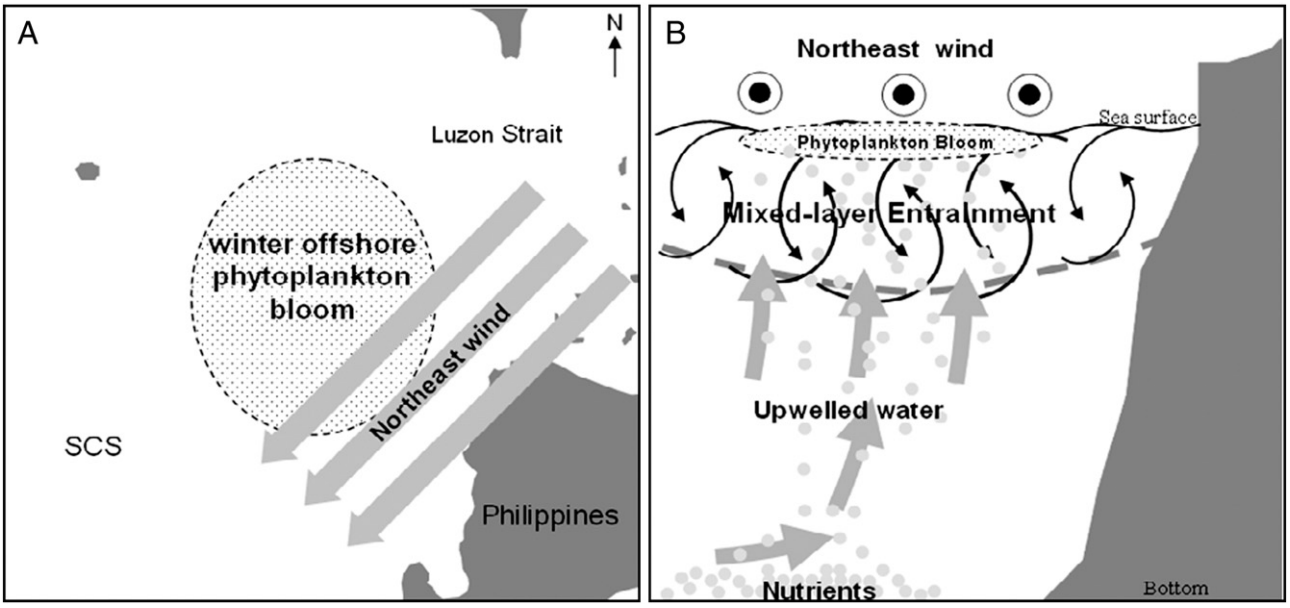


**Fig. 9.** Schematic diagram of the mechanisms responsible for the winter phytoplankton blooms (see text).

also appear in December and January (Fig. 5). The occurrence of phytoplankton blooms coincides with these periods of highest Ekman pumping and entrainment. The wind intensifies mixing, and increased entrainment brings nutrients which support the growth of phytoplankton from the subsurface upwelled water to the upper layer (Madhupratap et al., 1996). The homogeneous profiles of N, P and Si in the upper layer are consistent with vigorous mixing (Fig. 6B–D). The concentrations of N, P, and Si change slightly in the upper 50 m; dramatic increasing is evidenced below this layer.

*4.3.2. A conceptual model for bloom formation*

The schematic diagrams presented in Fig. 9 illustrate the mechanisms underlying the offshore winter phytoplankton bloom. During the winter northeast monsoon, the bloom appears to the right of the along-coast wind (Fig. 9A), which is suggestive of a coastal upwelling process. However, the upwelling is a subsurface phenomenon, which does not appear to cool SST or deliver nutrients to the mixed layer. How does the winter phytoplankton bloom occur in the study area? The strong wind stress results in Ekman pumping, which induces subsurface upwelling. Nutrients from the deep sea are transported toward the surface in upwelled waters. Stronger local wind stirring at the sea surface increases turbulent mixing, which causes entrainment of water from below. As the mixed layer deepens, turbulence entrains nutrients delivered by subsurface upwelling. Because the biological capacity for nutrient utilization exceeds the nutrient supply, nutrients remain low in the mixed layer. However, the nutrient flux appears to be sufficient to fuel the blooms observed in the region.

## 5. Conclusions

The region near Luzon Strait is oligotrophic in general, but it displays some unique features in wintertime. The present study reveals consistent wintertime phytoplankton blooms southwest of Luzon Strait. Two mechanisms underlying the winter phytoplankton blooms are Ekman pumping-driven subsurface upwelling and upper mixed layer entrainment.

Both the biological and physical processes in the study region are influenced by the wind. Nutrients are upwelled into the lower layer by subsurface upwelling induced by positive Ekman pumping. Local wind stirring subsequently entrains nutrients into the upper layer, fueling the observed plankton blooms. Our analysis has helped to elucidate the contributions of a few physical forcing mechanisms to biological processes in this region. However, hydrological characteristics and bottom topography are complex in the vicinity of Luzon Strait, and additional processes may be important. Seasonal variations of Kuroshio intrusions in this area result in more mesoscale eddies in winter than in summer (Wu and Chiang, 2007). Further study is needed to ascertain the degree to which mesoscale eddies could be involved in the formation of winter phytoplankton blooms in this area.

## Acknowledgements

This work was jointly supported by research projects awarded to Dr. D.L. Tang: (1) National Natural Sciences Foundation of China (40976091, 40811140533) and Guangdong Natural Science Foundation (8351030101000002); (2) Key Project of Knowledge Innovation Program, Chinese Academy of Sciences (KZCX2-YW-226; LYQY200701), (3) The CAS/SAFEA International Partnership Program for Creative Research Teams (KZCX2-YW-T001). The authors greatly appreciate data provided by others. We extend thanks to Prof. Dennis McGillicuddy, Prof. Ruixin Huang, Dr. Fei Wang, Dr. Xinfeng Zhang, and anonymous reviewers for their valuable help and comments on this study.

## References

Alexander, M.A., 1992. Midlatitude atmosphere–ocean interaction during El Niño. Part I: the North Pacific Ocean. J. Climate 5, 944–958.
Antonov, J.I., Locarnini, R.A., Boyer, T.P., Mishonov, A.V., Garcia, H.E., 2006. World Ocean Atlas 2005, 2: salinity. In: Levitus, S. (Ed.), NOAA Atlas NESDIS, 62. U.S. Government Printing Office, Washington, D.C., p. 182.
Backhaus, J.O., et al., 2003. Convection and primary production in winter. Mar. Ecol. Prog. Ser. 251, 1–14.
Botsford, L.W., Lawrence, C.A., Dever, E.P., Hastings, A., Largier, J., 2006. Effects of variable winds on biological productivity on continental shelves in coastal upwelling systems. Deep Sea Res. Part II 53 (25–26), 3116–3140.
Chao, S.-Y., Shaw, P.-T., Wu, S.-Y., 1996. Deep water ventilation in the south China Sea. Deep Sea Res. Part I 43, 445–466.
Chen, C.T.A., Liu, K.-K., MacDonald, R.W., 2003. Continental margin exchanges. In: Fasham, M.J.R. (Ed.), Ocean Biogeochemistry: The Role of the Ocean Carbon Cycle in Comparison with the West Philippine Sea: Terrestrial, Atmospheric and Oceanic Sciences, 3, pp. 587–602.
Chen, C.-C., Shiah, F.-K., Chung, S.-W., Liu, K.-K., 2006. Winter phytoplankton blooms in the shallow mixed layer of the South China Sea enhanced by upwelling. J. Mar. Sys. 59 (1–2), 97–110.

Chen, Y.L.L., Chen, H.-Y., Lin, I.-I., Lee, M.-A., Cheng, J., 2007. Effects of cold eddy on phytoplankton production and assemblages in Luzon Strait bordering the South China Sea. J. Oceanogr. 63, 671–683.
Collins, C.A., Pennington, J.T., Castro, C.G., Rago, T.A., Chavez, F.P., 2003. The California Current system off Monterey, California: physical and biological coupling. Deep Sea Res. Part II 50 (14–16), 2389–2404.
Dwivedi, R.M., Raman, M., Babu, K.N., Singh, S.K., Vyas, N.K., Matondkar, S.G.P., 2008. Formation of algal bloom in the northern Arabian Sea deep waters during January–March: a study using pooled in situ and satellite data. Int. J. Remote Sens. 29 (15), 4537–4551.
Emilie, T.K., Francis, M., 2009. Patterns of variability of sea surface chlorophyll in the Mozambique Channel: a quantitative approach. J. Mar. Sys. 77 (1–2), 77–88.
Farris, A., Wimbush, M., 1996. Wind-induced Kuroshio intrusion into the South China Sea. J. Oceanogr. 52, 771–784.
Garcia, H.E., Locarnini, R.A., Boyer, T.P., Antonov, J.I., 2006a. World Ocean Atlas 2005, 3: dissolved oxygen, apparent oxygen utilization, and oxygen saturation. In: Levitus, S. (Ed.), NOAA Atlas NESDIS, 63. U.S. Government Printing Office, Washington, D.C., p. 342.
Garcia, H.E., Locarnini, R.A., Boyer, T.P., Antonov, J.I., 2006b. World Ocean Atlas 2005, 4: nutrients (phosphate, nitrate, silicate). In: Levitus, S. (Ed.), NOAA Atlas NESDIS, 64. U.S. Government Printing Office, Washington, D.C., p. 396.
Hardy, D.M., 1977. Empirical eigenvector analysis of vector observations. Geophys. Res. Lett. 4, 319–320.
Hayes, D.E., Lewis, S.D., 1984. A geophysical study of the Manila trench, Luzon, Philippines. 1. Crustal structure, gravity and regional tectonic evolution. J. Geophys. Res. 89 (B11), 9171–9195.
Kutzbach, J.E., 1967. Empirical eigenvectors of sea-level pressure, surface temperature and precipitation complexes over North America. J. Appl. Meteorol. 6, 791–802.
Labiosal, R.G., Arrigo, K.R., 2003. The interplay between upwelling and deep convective mixing in determining the seasonal phytoplankton dynamics in the Gulf of Aqaba: evidence from SeaWiFS and MODIS. Limnol. Oceanogr. 48 (6), 2355–23368.
Liu, A.-K., Hsu, M.-K., 2003. Nonlinear internal wave study in the South China Sea using SAR. Int. J. Remote Sens. 25, 1–5.
Locarnini, R.A., Mishonov, A.V., Antonov, J.I., Boyr, T.P., Garcia, H.E., 2006. World Ocean Atlas 2005, 1: temperature. In: Levitus, S. (Ed.), NOAA Atlas NESDIS, 61. U.S. Government Printing Office, Washington, D.C., p. 182.
Lorenz, E.N., 1956. Empirical Orthogonal Functions and Statistical Weather Prediction, Scientific Report I, Statistical Forecasting Project. Mass. Inst. Tech., Cambridge, p. 49.
Madhupratap, M., Kumar, S.P., Bhattathiri, P.M.A., Kumar, M.D., Raghukumar, S., Nair, K.K.C., Ramaiah, N., 1996. Mechanism of the biological response to winter cooling in the northeastern Arabian Sea. Nature 384 (6609), 549–552.
Martin, M.C., Villanoy, C.L., 2008. Sea Surface Variability of Upwelling Area Northwest of Luzon, Philippines, Dynamic Planet. Springer, Berlin Heidelberg, pp. 84–87.
McGillicuddy Jr., D.J., Robinson, A.R., 1997. Eddy-induced nutrient supply and new production in the Sargasso Sea. Deep-Sea Res. Part I 44, 1427–1450.
McGillicuddy Jr., D.J., Robinson, A.R., Siegel, D.A., Jannasch, H.W., Johnson, R., Dickey, T.D., McNeil, J., Michaels, A.F., Knap, A.H., 1998. Influence of mesoscale eddies on new production in the Sargasso Sea. Nature 394, 283–286.
McGillicuddy Jr., D.J., Johnson, R., Siegel, D.A., Michaels, A.F., Bates, N.R., Knap, A.H., 1999. Mesoscale variations of biogeochemical properties in the Sargasso Sea. J. Geophys. Res. 104, 13381–13394.
Mendoza, V.M., Villanueva, E.E., Adem, J., 2005. On the annual cycle of the sea surface temperature and the mixed. Atmõsfera 18 (2).
Nezlin, N.P., McWilliams, J.C., 2003. Satellite data, Empirical Orthogonal Functions, and the 1997–1998 El Niño off California. Remote Sens. Environ. 84 (2), 234–254.
Peliz, A.J., Fiúza, A.F.G., 1999. Temporal and spatial variability of CZCS-derived phytoplankton pigment concentrations off the western Iberian Peninsula. Int. J. Remote Sens. 20 (7), 1363–1403.
Peñaflor, E.L., Villanoy, C.L., Liu, C.-T., David, L.T., 2007. Detection of monsoonal phytoplankton blooms in Luzon Strait with MODIS data. Remote Sens. Environ. 109 (4), 443–450.
Qu, T., 2000. Upper-layer circulation in the South China Sea. J. Phys. Oceanogr. 30, 1450–1460.
Radiarta, I.N., Saitoh, S.I., 2008. Satellite-derived measurements of spatial and temporal chlorophyll-*a* variability in Funka Bay, southwestern Hokkaido, Japan. Estuar. Coast. Shelf Sci. 79, 400–408.
Shaw, P.-T., Chao, S.-Y., 1994. Surface cirulation in the South China Sea. Deep Sea Res. Part I 41, 1663–1683.
Shaw, P.-T., Chao, S.-Y., Liu, K.-K., Pai, S.-C., Liu, C.-T., 1996. Winter upwelling off Luzon in the northeastern South China Sea. J. Geophys. Res. 101, 16435–16448.
Siegel, H., Ohde, T., Gerth, M., Lavik, G., Leipe, T., 2007. Identification of coccolithophore blooms in the SE Atlantic Ocean off Namibia by satellites and in-situ methods. Cont. Shelf Res. 27 (2), 258–274.
Steinberg, D.K., et al., 2001. Overview of the US JGOFS Bermuda Atlantic Time-series Study (BATS): a decade-scale look at ocean biology and biogeochemistry. Deep Sea Res. Part II 48 (8–9), 1405–1447.
Stewart, R.H., 2008. Introduction to Physical Oceanography. Texas A & M University, Texas, pp. 133–147.
Strang, E.J., Fernando, H.J.S., 2001. Entrainment and mixing in stratified shear flows. J. Fluid Mech. 428, 349–386.
Tang, D.L., Ni, I.H., Kester, D.R., 1999. Remote sensing observations of winter phytoplankton blooms southwest of the Luzon Strait in the South China Sea. Mar. Ecol. Prog. Ser. 191, 43–51.
Tang, D.L., Kawamura, H., Luis, A.J., 2002. Short-term variability of phytoplankton blooms associated with a cold eddy in the northwestern Arabian Sea. Remote Sens. Environ. 81 (1), 82–89.
Tang, D.L., Kawamura, H., Lee, M.-A., Van-Dien, T., 2003. Seasonal and spatial distribution of chlorophyll-*a* concentrations and water conditions in the Gulf of Tonkin, South China Sea. Remote Sens. Environ. 85 (4), 475–483.
Tang, D.L., Kawamura, H., Dien, T.V., Lee, M.A., 2004a. Offshore phytoplankton biomass increase and its oceanographic causes in the South China Sea. Mar. Ecol. Prog. Ser. 268, 31–41.
Tang, D.L., Kawamura, H., Doan-Nhu, H., Takahashi, W., 2004b. Remote sensing oceanography of a harmful algal bloom off the coast of southeastern Vietnam. J. Geophys. Res. 109.
Udarbe-Walker, M.J.B., Villanoy, C.L., 2001. Structure of potential upwelling areas in the Philippines. Deep Sea Res. Part I 48, 1499–1518.
Wang, B., Huang, F., Wu, Z., Yang, J., Fu, X., Kikuchia, K., 2009. Multi-scale climate variability of the South China Sea monsoon: a review. Dyn. Atmos. Oceans 47, 15–37.
Weare, B.C., Navato, A.R., Newell, R.E., 1976. Empirical orthogonal analysis of Pacific sea surface temperatures. J. Phys. Oceanogr. 6 (5), 671–678.
Wilkerson, F.P., Lassiter, A.M., Dugdale, R.C., Marchi, A., Hogue, V.E., 2006. The phytoplankton bloom response to wind events and upwelled nutrients during the CoOP WEST study. Deep Sea Res. Part I 53, 3023–3048.
Wu, C.-R., Chiang, T.-L., 2007. Mesocale eddies in the northern South China Sea. Deep Sea Res. Part II 54, 1575–1588.
Wyrtki, K., 1961. Physical oceanography of the Southeast Asia waters. NAGA Report 2, 1–195.